IVYSPRING INTERNATIONAL PUBLISHER

Theranostics

2018; 8(21): 6025-6034. doi: 10.7150/thno.26607

Research Paper

Hypoxia-triggered single molecule probe for high-contrast NIR II/PA tumor imaging and robust photothermal therapy

Xiaoqing Meng[1, 2], Jiali Zhang[1, 2], Zhihong Sun[1], Lihua Zhou[1], Guanjun Deng[1, 2], Sanpeng Li[1], Wenjun Li[1], Ping Gong[1, 2, 3]✉, Lintao Cai[1, 2]✉

1. Guangdong Key Laboratory of Nanomedicine, Shenzhen Engineering Laboratory of Nanomedicine and Nanoformulations, CAS Key Lab for Health Informatics, Shenzhen Institutes of Advanced Technology, Chinese Academy of Sciences, Shenzhen 518055, China.
2. University of Chinese Academy of Sciences, Beijing 100049, China
3. Guangdong Key Laboratory for Research and Development of Natural Drugs, Guangdong Medical University, Dongguan 523808, China

✉ Corresponding authors: Lintao Cai, Ping Gong, Guangdong Key Laboratory of Nanomedicine, Shenzhen Engineering Laboratory of Nano-medicine and Nanoformulations, CAS Key Lab for Health Informatics, Shenzhen Institutes of Advanced Technology, Chinese Academy of Sciences, Shenzhen 518055, China. Tel: +86-0755-86392210; Fax: +86-755-86585222; E-mail: lt.cai@siat.ac.cn, ping.gong@siat.ac.cn.

Received: 2018.04.11; Accepted: 2018.07.06; Published: 2018.11.15

Abstract

Hypoxia is a common characteristic of solid tumors. This important feature is associated with resistance to radio-chemotherapy, which results in poor prognosis and probability of tumor recurrence. Taking advantage of background-free NIR II fluorescence imaging and deeper-penetrating photoacoustic (PA) imaging, we developed a hypoxia-triggered and nitroreductase (NTR) enzyme-responsive single molecule probe for high-contrast NIR II/PA tumor imaging and hypoxia-activated photothermal therapy (PTT), which will overcome cellular resistance during hypoxia.

Methods: The single molecule probe IR1048-MZ was synthesized by conjugating a nitro imidazole group as a specific hypoxia trigger with an IR-1048 dye as a NIR II/PA signal reporter. We investigated the NIR II fluorescence, NIR absorbance and photothermal effect in different hypoxia conditions *in vitro*, and performed NIR II/PA tumor imaging and hypoxia-activated photothermal therapy in mice.

Results: This versatile molecular probe IR1048-MZ not only realized high-contrast tumor visualization with a clear boundary by NIR II fluorescence imaging, but also afforded deep-tissue penetration at the centimeter level by 3D PA imaging. Moreover, after being activated by NTR that is overexpressed in hypoxic tumors, the probe exhibited a significant photothermal effect for curative tumor ablation with no recurrence.

Conclusions: We have developed the first hypoxia-triggered and NTR enzyme-responsive single molecule probe for high-contrast NIR II/PA tumor imaging and hypoxia-activated photothermal therapy. By tracing the activity of NTR, IR1048-MZ may be a promising contrast agent and theranostic formulation for other hypoxia-related diseases (such as cancer, inflammation, stroke, and cardiac ischemia).

Key words: hypoxia-triggered, single molecule probe, NIR II fluorescence imaging, PA imaging, activatable photothermal therapy.

Introduction

Hypoxia is a common characteristic of solid tumors [1-3]. This important feature is associated with resistance to radio-chemotherapy, which results in poor prognosis and probability of tumor recurrence

[4-12]. Therefore, there is a need to monitor tumor hypoxia for assessing the aggressiveness of tumors and predicting the outcome of therapy. Since hypoxia can cause overexpression of nitroreductase (NTR) and NTR level is directly related to the degree of hypoxia [13-14], NTR is considered an indicative biomarker of hypoxia and its level can be used to evaluate the hypoxic degree of a tumor [14-16]. Under hypoxic conditions, NTR can catalyze the reduction of nitro compounds to the corresponding amine compounds in the presence of NADH as an electron donor [17-20]. Such an enzyme-catalyzed reduction has been recognized to be a useful reaction for the design of hypoxia probes.

There are currently several fluorescence probes for tumor hypoxia detection [21-25]. However, all of these fluorescence probes operate in the visible or NIR I region (700–900 nm). Recent studies have demonstrated that the new NIR II window (1000–1700 nm) is advantageous for biological imaging, with improved spatial resolution, a higher signal-to-noise ratio, and deeper tissue penetration depth, owing to reduced photon scattering and autofluorescence in the NIR II range [26-29]. But, most studies in the NIR II window have focused on developing new image contrast agents for bioimaging, such as inorganic nanomaterials (single-walled carbon nanotubes, metal chalcogenide QDs, rare-earth nanoparticles), polymer nanoparticles (pDA), and organic small-molecule dyes (e.g., IR1061, CH1055, IR-FE, IR-FEP) [30]. To date, only a few studies have focused on NIR II diagnostic sensors, and there are no available NIR II probes for tumor hypoxia detection [31].

Hypoxia has been widely reported to cause chemo- or radiation-resistance, which significantly undermine the efficacy of cancer therapies [4-6, 32-33]. So, therapies overcoming cellular resistance during hypoxia are of great importance. Phototherapies, including photodynamic therapy (PDT) and photothermal therapy (PTT), have been introduced into clinical trials for cancer therapy because of their advantages for improving the anti-tumor effect by overcoming multidrug resistance [34-36], with reduced side effects. Actually, several PDT photosensitizers have been approved by the US Food and Drug Administration (FDA) for the treatment of some specific indications [37]. Nevertheless, PDT is highly dependent on oxygen, thus it is not effective in the hypoxic environment of cancer. In contrast, PTT, as a new therapeutic technology, is not affected by the hypoxia in tumors [38-40]. However, the currently available PTT photosensitizers generally lack selectivity, which leads to indiscriminate heating of both tumor tissue and normal tissues during treatment, possibly causing burn injuries in normal tissues. Therefore, exploring PTT agents that can be activated by the hypoxic tumor microenvironment would be much more attractive.

Herein, we aimed to develop a novel NTR enzyme-responsive single molecule probe for high-contrast NIR II/PA tumor imaging and hypoxia-activated photothermal therapy (**Figure 1**). A simple and well-designed small-molecule IR1048-MZ was synthesized by conjugating a nitro imidazole group (2-(2-nitroimidazolyl)ethylamine, MZ) with an IR-1048 dye in the NIR II window. The electron-withdrawing MZ group induces electron-transfer, which subsequently results in fluorescence quenching and decreases the absorbance of IR-1048 [41-43]. When the MZ group was reduced by NTR [44-50] to the corresponding amine group, the NIR II fluorescence and photoacoustic PA signal of IR1048-MZ were recovered. Thus, as a NIR II/PA sensor, IR1048-MZ enables the selective detection of local NTR concentrations. Furthermore, the NIR II/PA probe can be used to pinpoint a tumor and monitor tumor hypoxia. Notably, strongly amplified photothermal efficacy was also activated simultaneously by the enhanced absorption in the NIR I region that was triggered by NTR. The imaging and PTT results in mice bearing tumor xenografts demonstrated that IR1048-MZ could be used to visualize tumors with a clear boundary and deep tissue penetration and function as an efficient NTR-activated photosensitizer with minimum damage to normal tissues. This successful hypoxia-triggered NIR II fluorescence/NIR-PA/NIR-PTT turn-on system provides a new strategy for the further design of theranostic probes for the simultaneous activation of multimodality imaging and phototherapy.

Results and Discussion

Synthesis and characterization of IR1048-MZ molecular probe

IR1048-MZ was synthesized according to the routes depicted in **Figure S1**. The nuclear magnetic resonance (NMR) spectroscopy and high-resolution mass spectrometry (HRMS) data on the chemical characterization of the intermediates and the desired product are available in Supplementary Material. To demonstrate IR1048-MZH is the product of NTR-catalyzed IR1048-MZ in hypoxic conditions, HRMS and HPLC analyses were performed. Under hypoxia (0% pO_2), the HRMS spectrum of the reaction solution of IR1048-MZ with NTR showed a characteristic peak for IR1048-MZH at m/z = 741.3216 $[M + H]^+$ (**Figure S3B**). Whereas, under normoxia (20% pO_2), the HRMS spectrum of the reaction

solution showed no characteristic peak for IR1048-MZH (**Figure S3A**). These results verified that NTR catalyzed the reduction of IR1048-MZ to IR1048-MZH under hypoxia. Meanwhile, IR1048-MZH was further verified as a major final product by HPLC analysis. As shown in **Figure S4**, standard samples of NADH, NTR, IR1048-MZ, and IR1048-MZH all showed different peaks at 5.36, 8.39, 12.82, and 15.81 min distinctly. When IR1048-MZ was mixed with NTR in the presence of NADH under hypoxia (0% pO_2), a new peak at 15.81 min corresponding to IR1048-MZH was also observed, concomitant with a reduction in the peak at 12.82 min representing IR1048-MZ in the HPLC trace (**Figure S4F**). While under normoxia (20% pO_2), the HPLC spectrum of the reaction solution showed no characteristic peak for IR1048-MZH (**Figure S4E**). All of these results confirmed the deduced mechanism of the conversion of IR1048-MZ into IR1048-MZH in the presence of NTR under hypoxia.

Theoretical calculations in **Figure 1** demonstrated that the bandgap between the highest occupied molecular orbital (HOMO) and the lowest unoccupied molecular orbital (LUMO) of IR1048-MZ was 2.572. But, the HOMO-LUMO bandgap of IR1048-MZH was 2.236, which was lower than that of IR1048-MZ. These data suggested the electron-transfer process in IR1048-MZH was suppressed by the reduction of IR1048-MZ and resulted in enhanced emission intensity. Subsequently, to verify the sensitivity of IR1048-MZ to NTR, we first analyzed the absorption and fluorescence spectra of IR1048-MZ in the presence and absence of NTR *in vitro*. The probe showed a very weak absorption in the range of 900–1060 nm. However, after being reduced by NTR, it produced a maximum absorption peak at about 980 nm (**Figure 2A**). Moreover, as shown in **Figure 2B**, probe IR1048-MZ had almost no fluorescence emission at 1046 nm with a low fluorescence quantum yield (ΦF) of 1.88×10^{-5}, but its reaction solution with NTR exhibited as much as a 106.9-fold enhancement at 1046 nm (ΦF = 0.006). The maximum excitation and emission wavelengths of probe IR1048-MZ were 980 nm and 1046 nm, respectively. The calculated Stokes shift between the excitation and emission reached 66 nm. Such a large shift can improve the sensitivity of probe IR1048-MZ, which is a desired characteristic in probe design. Importantly, the introduction of a hydrophilic 2-nitroimidazole into the probe also greatly improved the probe's aqueous solubility, thus make it suitable for biological systems (**Figure S8** and **Figure S9**).

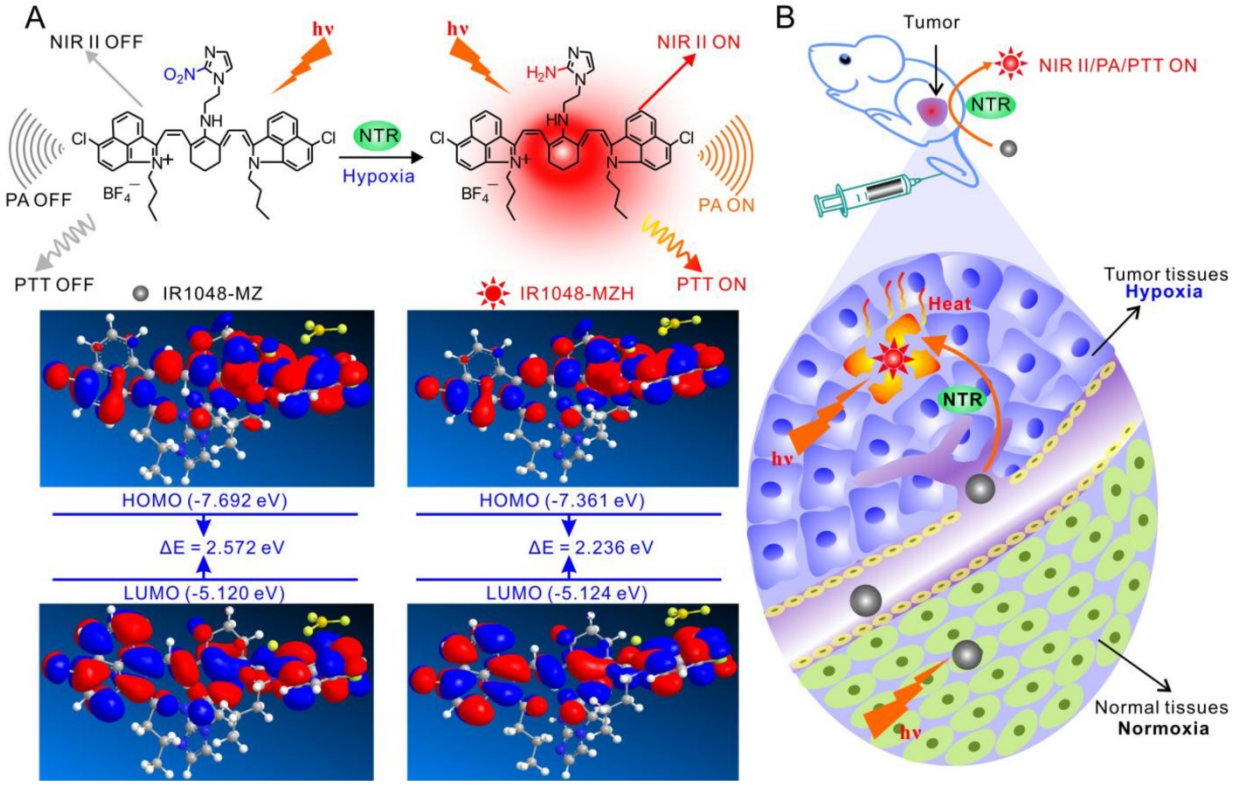

Figure 1. Schematic illustration of the NTR-responsive NIR II fluorescence/PA probe for visualizing tumors and inducing an NTR-triggered PTT effect. (A) Catalyzed mechanism of IR1048-MZ activated by NTR. Frontier molecular diagram profiles of IR1048-MZ and IR1048-MZH. **(B)** The NIR II/PA/PTT of IR1048-MZ is quenched in the vessels and normal tissues. In contrast, the NIR II/PA/PTT of IR1048-MZ is activated by NTR when meeting cancer cells and hypoxic tumors.

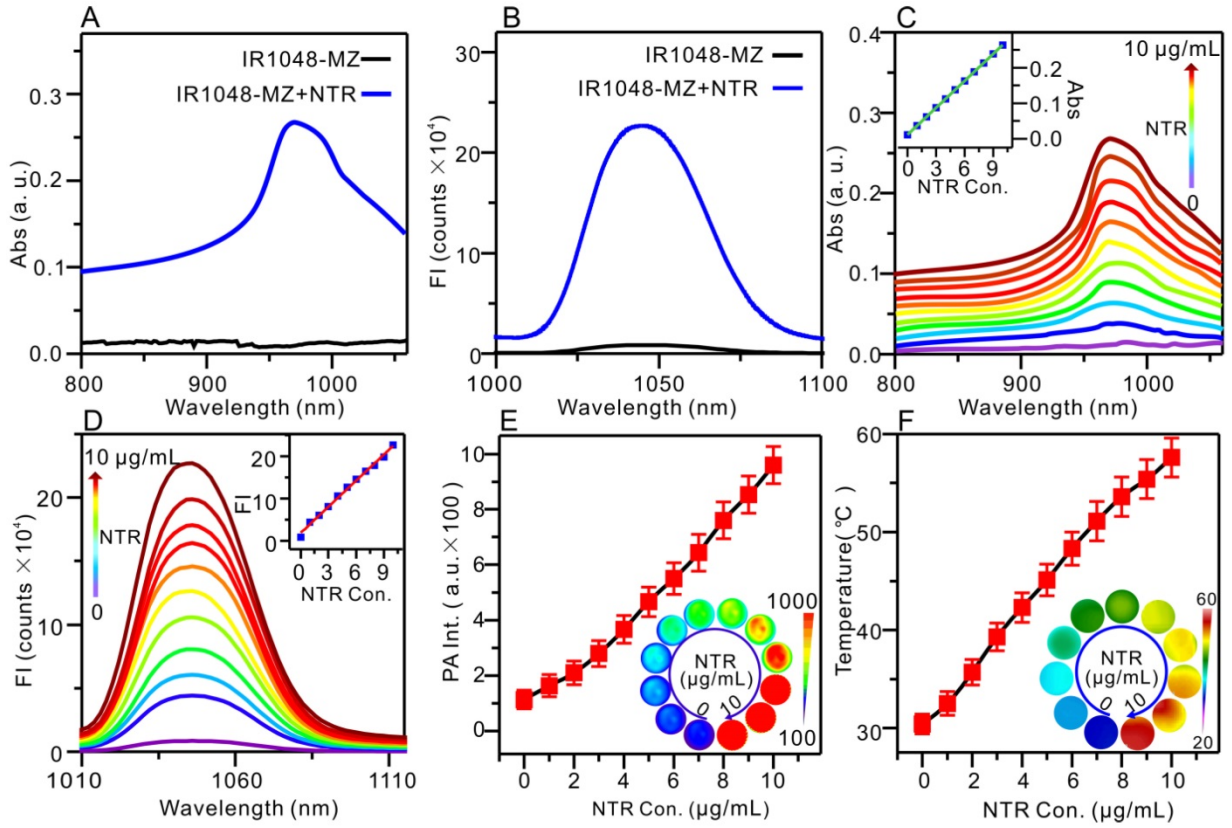

Figure 2. Absorption (Abs)/NIR II fluorescence /PA/PTT responses of IR1048-MZ to NTR *in vitro* with 500 μM NADH as a coenzyme. (A) Absorption spectra in the absence (black) and presence (blue) of NTR. **(B)** Fluorescence emission spectra (λ_{ex} /λ_{em} = 980/1046 nm) in the absence (black) and presence (blue) of NTR; FI: fluorescence intensity. **(C)** Absorption responses of 5 μg/mL IR1048-MZ to different concentrations of NTR. Inset: a linear correlation between absorption intensity and concentration of NTR. **(D)** NIR II fluorescence responses of 5 μg/mL IR1048-MZ to different concentrations of NTR. Inset: a linear correlation between emission intensity and concentration of NTR. **(E)** PA responses of 5 μg/mL IR1048-MZ to different concentrations of NTR; PA Int.: PA intensity. Inset: PA imaging of 5 μg/mL IR1048-MZ solution with different concentrations of NTR. The impulse excitation wavelength was 880 nm. **(F)** PT responses of 5 μg/mL IR1048-MZ to different concentrations of NTR after 980 nm NIR laser irradiation (0.1 W/cm²) for 2 min. Inset: infrared thermal imaging of 5 μg/mL IR1048-MZ solution with different concentrations of NTR after NIR laser irradiation for 2 min.

With increasing NTR concentration from 0 to 10 μg/mL, the absorption peak (980 nm) intensity of IR1048-MZ increased linearly (**Figure 2C**). The fluorescence intensity of IR1048-MZ after reacting with different NTR concentrations is also illustrated in **Figure 2D**. The increase in NTR concentration resulted in an increase in the fluorescence intensity of the probe at 1046 nm (λ_{ex} = 980 nm). Moreover, there was a good positive linear relationship between NTR (0–10 μg/mL) and the fluorescence intensity of the probe (F = 18675 + 20631 × [NTR] μg/mL, R = 0.9939). The detection limit value of NTR was found to be 43 ng/mL. The fluorescence kinetic curve of IR1048-MZ and NTR depicted in **Figure S10** indicated that higher concentration of NTR resulted in a stronger fluorescence intensity and faster response. The increases in NIR absorption of the probe after reaction with NTR lead to a strong PA signal and high thermal efficacy. The NTR-activated PA imaging and PT imaging *in vitro* are presented in **Figure 2E** and **Figure 2F**, respectively. As the NTR concentration was increased from 0 to 10 μg/mL, the PA signal increased linearly from 121 to 936, and the temperature of the solutions after 980 nm NIR laser irradiation (0.1 W/cm²) for 2 min also increased from 30.4 °C to 57.6 °C. The photothermal conversion efficiency was measured to be 20.2 %, approximately 5.5-fold higher than the value reported for ICG (~3.1%) [37]. Having excellent responsiveness to NTR, 1048-MZ also works steadily in pH 6.0–8.0 (**Figure S12A**) or in the presence of various bioactive molecules (**Figure S12B**). The high selectivity expands the applications of IR1048-MZ in complex intracellular environments. These *in vitro* experiments indicated that the NIR II fluorescence, PA, and PT were activated by NTR simultaneously and that IR1048-MZ is a promising theranostic agent that can be used for hypoxia-activated imaging and therapy *in vivo*.

NIR II fluorescence imaging of tumor hypoxia with IR1048-MZ *in vivo*

Fluorescence imaging of animals in the NIR II window dramatically benefits from deeper penetration due to minimal autofluorescence and reduced scattering of photons that is inversely

proportional to wavelength as ~ λ^{w} (w = 0.22–1.68) in biological systems [51-54]. In the next step, the feasibility of NIR II fluorescence imaging of tumors with IR1048-MZ was investigated by intravenous injection of IR1048-MZ into BALB/c nude mice bearing subcutaneous A549 tumor, which is known to express NTR under hypoxic conditions [55-56]. The NIR II fluorescence signal in the tumor tissue was clearly visible at 10 h post-injection (p.i.) and reached its maximum at about 14 h p.i. Notably, unlike with most of the reported probes, the *in vivo* NIR II fluorescence imaging of tumor hypoxia with IR1048-MZ did not result in an observable background signal (**Figure 3A-B**). The biodistribution of the probe was studied by measuring the probe content (total content of IR1048-MZ and IR1048-MZH) in different organs at various time points after intravenous injection of IR1048-MZ by inductively coupled plasma mass spectrometry (**Figure 3C**). We found that the highest accumulation of the probe occurred in the kidney at 5 h post-injection, indicating that the probe eliminated by renal excretion pathways from the animal body. *Ex vivo* NIR II fluorescence imaging of dissected tumor and organs obtained from the different groups of A549 tumor-bearing mice was performed after 14 h p.i. to further assess the characteristics of the probe (**Figure 3E-F**). High NIR II fluorescence intensity for IR1048-MZ was observed in the tumor, whereas the organs (heart, lung, liver, spleen, and kidneys) showed no detectable signal. The tumor-to-background ratio at 14 h p.i. was as much as 30 (**Figure 3D**), about 3.8 times that of the newly reported NTR-sensitive probe in the NIR I region [56]. The specific response to hypoxia and depression of autofluorescence makes IR1048-MZ an excellent background-free hypoxia probe for imaging tumors in mice with high contrast, thus made it superior to most of the reported probes.

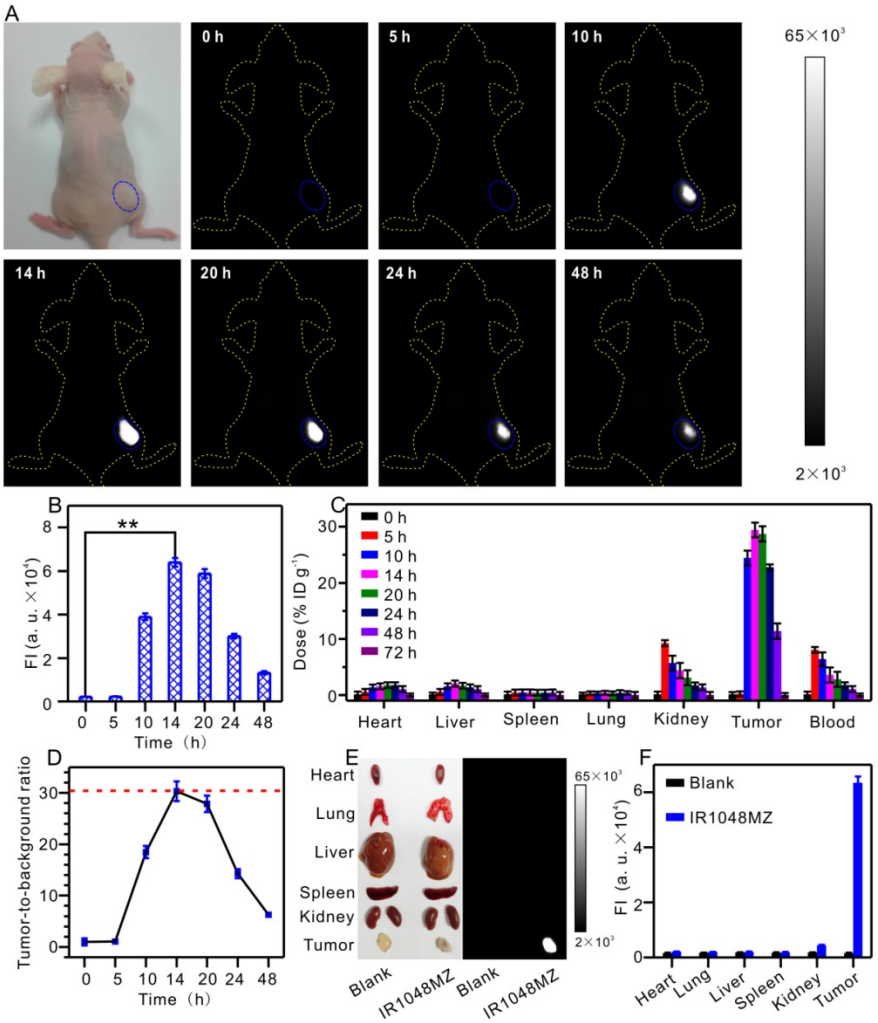

Figure 3. NIR II fluorescence imaging of tumor hypoxia *in vivo* after intravenous injection of 200 μL 40 μg/mL IR1048-MZ. All the NIR II images were acquired with a NIR II imaging system with 980 nm excitation and 1000 nm longpass emission filter. **(A)** NIR II fluorescence imaging of tumors (blue circles) in living mice at different time intervals and **(B)** quantified fluorescence intensities. **(C)** Probe content in the heart, liver, spleen, lung, kidney, tumor and blood of the mice at various time points after intravenous injection. The results are presented as the percentage of injected dose per gram of dissected tissue and averaged over five mice per group (mean ± s.d.). **(D)** The tumor-to-background ratio plotted as a function of time after intravenous injection for NIR II images. **(E)** *Ex vivo* NIR II fluorescence imaging of dissected tumors and organs from mice in different groups at 14 h post-injection and **(F)** quantified fluorescence intensities.

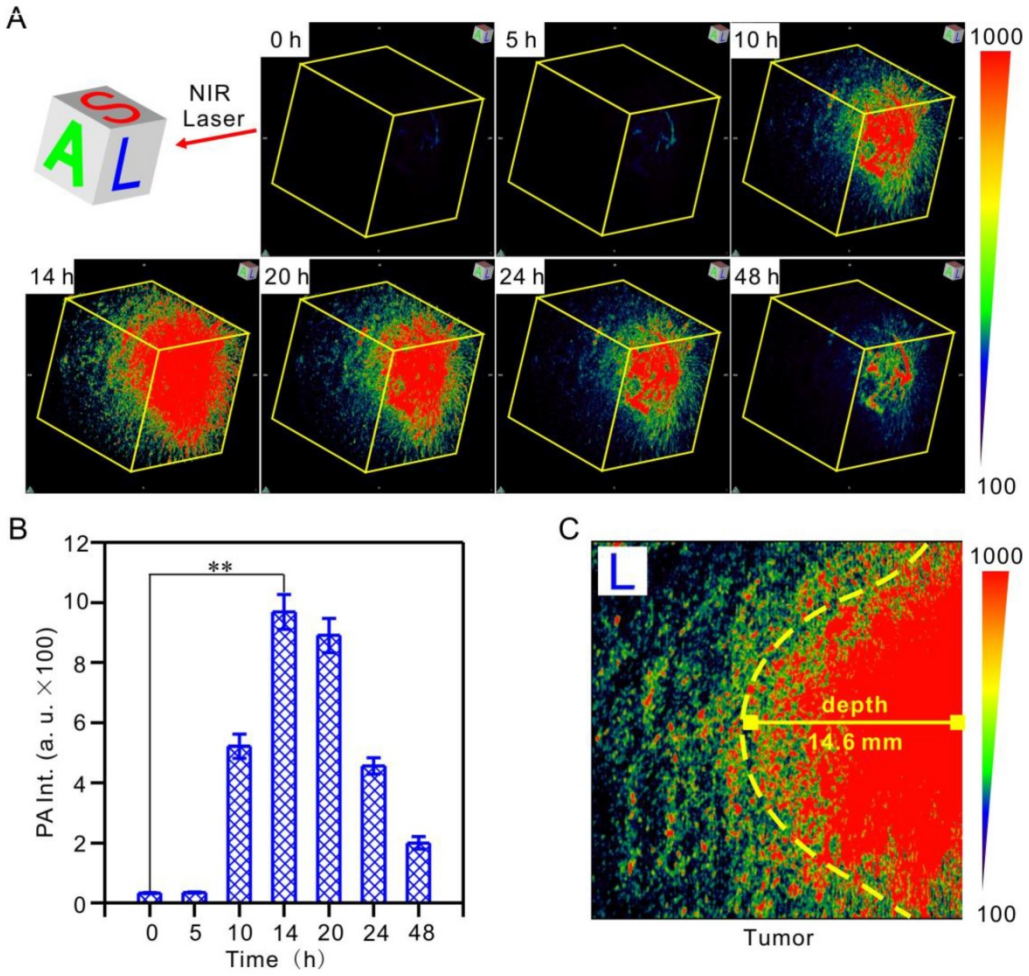

Figure 4. Hypoxia-activated 3D photoacoustic PA imaging of tumors *in vivo* after intravenous injection of 200 μL 40 μg/mL IR1048-MZ. The impulse excitation wavelength was 880 nm. **(A)** PA imaging of tumors in living mice at different time intervals and **(B)** quantified PA intensities. **(C)** Penetration depth of PA imaging in the longitudinal section (L) 14 h post-injection.

3D PA imaging of tumor hypoxia with IR1048-MZ *in vivo*

PA tomography offers dramatic benefits for imaging in live animals, providing high-resolution images at depths in the cm range, which has been recognized as a promising alternative to X-ray scans and MRI for clinical diagnosis [57-59]. It deserves to be mentioned that, for the first time, we realized hypoxic tumor detection by monitoring the 3D PA signal of IR1048-MZ with deep-tissue penetration and imaging *in vivo*. Hypoxia-activated PA imaging in A549 tumor-bearing BALB/c nude mice was carried out by tail vein injection of IR1048-MZ, and 3D PA signals at the tumor site at the indicated time points were recorded (**Figure 4A-B**). The 3D PA signals in the tumor regions were distinguishable at 10 h post-injection, reached their maximum value at about 14 h, and then began to decrease. This behavior agreed well with the NIR II fluorescence imaging results. Moreover, the penetration depth of the photoacoustic (PA) imaging in the longitudinal section (L) 14 h post-injection was up to 14.6 ± 0.2 mm (**Figure 4C**), which demonstrated that hypoxia-activated PA imaging provided deep tissue penetration and high spatial resolution. Considering the results from NIR II fluorescence and PA imaging in tumor-bearing mice, IR1048-MZ definitely serves as a specific hypoxia-activated NIR II/ PA imaging probe for accurate detection of the boundary and depth of tumors.

Hypoxia-activated PTT of tumor with IR1048-MZ in mice

Considering that the NIR absorption of the probe increased significantly in the presence of the overexpressed NTR in hypoxic tumors, we supposed that this single molecule probe, apart from serving as a NIR II/PA imaging probe, could be used as a hypoxia-activated photothermal agent for tumor photothermal ablation *in vivo*. First, to verify that the photothermal effect was selectively caused by hypoxia *in vivo*, an inhibition test of hypoxia with dicoumarin (an inhibitor of endogenous

nitroreductase) was performed [56, 60]. 100 μL dicoumarin solution (0.2 mM) was injected into tumor 1 on the left hind leg while tumor 2 on the right hind leg was untreated, and the mouse was then injected with 200 μL of IR1048-MZ (40 μg/mL) via the tail vein (**Figure 5A**). 14 h after the injection, both tumor 1 and tumor 2 were irradiated under 980 nm NIR laser (0.1 W/cm^2) for 2 min. Then infrared thermal imaging was performed. As demonstrated in **Figure 5A**, remarkably, the temperature of tumor 2 increased from 30 °C to 58 °C, which was sufficient to kill cancer cells, but the temperature of tumor 1 was still at 30 °C. Subsequently, to demonstrate that the NTR level in the tumor was down-regulated by the injection of the inhibitor (dicoumarin), a commercial hypoxyprobe (pimonidazole antibody, PIMO) immunofluorescence assay was carried out on tumor slices [61-63]. As shown in **Figure 5B**, the untreated group exhibited strong green fluorescence, which indicated that the untreated tumor was hypoxic with high levels of NTR. But, the group treated with the inhibitor exhibited weak fluorescence, which suggested that the NTR level was successfully down-regulated by the inhibitor. These results verified that the photothermal effect of the probe was selectively activated by hypoxia *in vivo*, indicating that the hypoxia-triggered photothermal sensitizer, which is specifically activated by tumor, renders the sensitizer maximal therapeutic efficacy and minimal side effects to normal tissues.

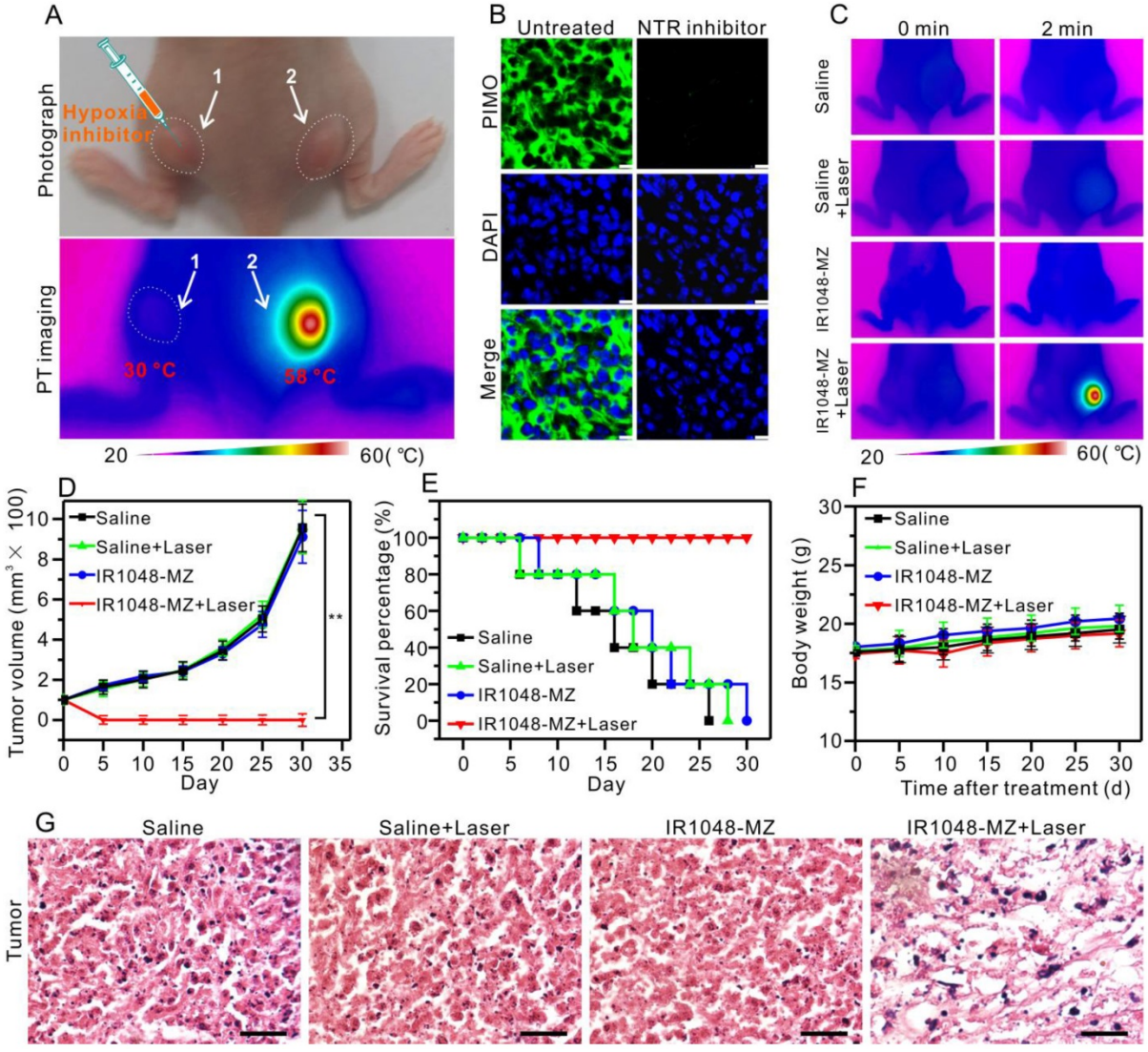

Figure 5. Hypoxia-activated photothermal therapy with IR1048-MZ in A549 tumor-bearing mice (injection dose: 200 μL 40 μg/mL). (A) Photograph and infrared thermal imaging of a mouse with two A549 tumors on the left and right hind legs 14 h after intravenous injection of IR1048-MZ. The room temperature was 23 °C. Tumor 1 was injected with dicoumarin as an inhibitor of NTR; Tumor 2 was without treatment. **(B)** Frozen sections of the tumor with or without injection of the NTR inhibitor (coumarin) stained with PIMO (green fluorescence) and DAPI (blue fluorescence); bars: 25 μm. **(C)** Infrared thermal imaging of the A549 tumor-bearing mice injected with saline or IR1048-MZ with or without 980 nm NIR laser irradiation (0.1 W/cm^2) for 2 min. The room temperature was 23 °C. **(D)** The A549 tumor growth curves over 30 d after treatment with 200 μL saline or 200 μL IR1048-MZ (40 μg/mL) with or without NIR laser irradiation (980 nm, 0.1 W/cm^2, 2 min). **(E)** The survival rate of A549 tumor-bearing mice after treatment. n = 5, ** P < 0.01. **(F)** The body weight variation of A549 tumor-bearing mice after treatment. n = 5, ** P < 0.01. **(G)** H&E staining of tumor regions from the different groups; bars: 50 μm.

Next, the treatment outcome of hypoxia-activated PTT with IR1048-MZ was evaluated in A549 tumor-bearing mice. As shown in the infrared thermal imaging results (**Figure 5C**), for the mice treated with IR1048-MZ and 980 nm laser irradiation at a low irradiance of 0.1 W/cm², their surface temperature increased quickly from ~30 °C to ~57 °C within 2 min. Conversely, the temperatures of tumors in the other groups without the hypoxia-dependent NIR absorbance under the same laser irradiation displayed little change. At 5 d after the PTT treatment, the tumors in the IR1048-MZ plus NIR laser irradiation group disappeared, and no tumor relapse was found from day 5 to day 30. In contrast, the tumors in the other groups showed rapid growth (**Figure 5D**). In addition, the survival rate of the mice treated with IR1048-MZ with NIR laser irradiation was 100% after 30 d, which was a significant improvement compared with those of the other groups (**Figure 5E**). The body weights of these experimental groups were not significantly different from that of the control group, indicating that the treatments were reasonably well-tolerated (**Figure 5F**). Additionally, the major blood indexes and liver-function indexes of mice injected with IR1048-MZ (**Table S1**) show no obvious abnormity or difference when compared with those of mice in the control group, further demonstrating the high biocompatibility of IR1048-MZ. Furthermore, tumor sections from the different groups were examined with a hematoxylin and eosin (H&E) staining assay. In **Figure 5G**, a morphology characteristic of apoptotic cells was observed in the H&E-stained tumors treated with IR1048-MZ and NIR laser irradiation, but this morphology was not observed in the other three groups. These results demonstrated that IR1048-MZ is safe and has great potential for use in hypoxia-activated PTT of tumors with high efficiency *in vivo*.

Conclusions

In summary, we have developed the first hypoxia-triggered and NTR enzyme-responsive single molecule probe for high-contrast NIR II/PA tumor imaging and hypoxia-activated photothermal therapy. The IR1048-MZ molecular probe itself has a very weak NIR II and PA signal. However, after activation in hypoxic tumors, the probe emits intense NIR II fluorescence and PA signal, which provided more accurate and deeper tissue imaging of the position and boundary of tumors. Importantly, the hypoxia-activated photothermal therapy of IR1048-MZ exhibited outstanding phototherapy efficacy with rapid increases in temperature and resulted in ablation of tumors with no recurrence. Therefore, the versatile IR1048-MZ probe was not only an activable NIR II/PA imaging probe with rapid, selective, and sensitive hypoxia response, but also a robust small-molecule photosensitizer for photothermal therapy. By tracing the activity of NTR, IR1048-MZ may be a promising contrast agent and theranostic formulation for hypoxia-related diseases (such as cancer, inflammation, stroke, and cardiac ischemia).

Abbreviations

NIR: near infrared; PA: photoacoustic; NTR: nitroreductase; PTT: photothermal therapy; PDT : photodynamic therapy; QDs: quantum dots; FDA: food and drug administration; MZ: (2-(2-nitroimidazolyl)ethylamine; NMR: nuclear magnetic resonance; HRMS: high-resolution mass spectrometry; HPLC: high performance liquid chromatography; HOMO: the highest occupied molecular orbital; LUMO: the lowest unoccupied molecular orbital; ΦF: fluorescence quantum yield; L: longitudinal section; PIMO: pimonidazole antibody; H&E: hematoxylin and eosin.

Supplementary Material

Supplementary figures and tables.
http://www.thno.org/v08p6025s1.pdf

Acknowledgment

This study was supported by the Key International S&T Cooperation Project (2015DFH 50230), National Natural Science Foundation of China (No. 21404115, 21375141, 51502333, 31571013, 81371679, 81401509, 81501580, and 81671758), Guangdong Natural Science Foundation of Research Team (2016A030312006), and Shenzhen Science and Technology Program (JCYJ20160429191503002, JCYJ20150521094519473, JCYJ20150403091443298, and JSGG20160331185422390).

Competing Interests

The authors have declared that no competing interest exists.

References

1. Pouyssegur J, Dayan F, Mazure NM. Hypoxia signalling in cancer and approaches to enforce tumour regression. Nature. 2006; 441: 437-43.
2. Jain RK. Normalization of Tumor Vasculature: An Emerging Concept in Antiangiogenic Therapy. Science. 2005; 307: 58-62.
3. Wilson WR, Hay MP. Targeting hypoxia in cancer therapy. Nat Rev Cancer. 2011; 11: 393-410.
4. Semenza GL. Intratumoral hypoxia, radiation resistance, and HIF-1. Cancer Cell. 2004; 5: 405-6.
5. Thienpont B, Steinbacher J, Zhao H, D'Anna F, Kuchnio A, Ploumakis A, et al. Tumour hypoxia causes DNA hypermethylation by reducing TET activity. Nature. 2016; 537: 63-8.
6. Facciabene A, Peng X, Hagemann IS, Balint K, Barchetti A, Wang L-P, et al. Tumour hypoxia promotes tolerance and angiogenesis via CCL28 and Treg cells. Nature. 2011; 475: 226-30.

7. Taylor CT, Colgan SP. Hypoxia and gastrointestinal disease. J Mol Med. 2007; 85: 1295-300.
8. Liu J, Liu Y, Bu W, Bu J, Sun Y, Du J, et al. Ultrasensitive Nanosensors Based on Upconversion Nanoparticles for Selective Hypoxia Imaging in Vivo upon Near-Infrared Excitation. J Am Chem Soc. 2014; 136: 9701-9.
9. Fan W, Bu W, Zhang Z, Shen B, Zhang H, He Q, et al. X-ray Radiation-Controlled NO-Release for On-Demand Depth-Independent Hypoxic Radiosensitization. Angew Chem Int Ed Engl. 2015; 54: 14026-30.
10. Brahimi-Horn MC, Chiche J, Pouysségur J. Hypoxia and cancer. J Mol Med. 2007; 85: 1301-7.
11. Shohet RV, Garcia JA. Keeping the engine primed: HIF factors as key regulators of cardiac metabolism and angiogenesis during ischemia. J Mol Med. 2007; 85: 1309-15.
12. Tuder RM, Yun JH, Bhunia A, Fijalkowska I. Hypoxia and chronic lung disease. J Mol Med. 2007; 85: 1317-24.
13. Brown JM, Wilson WR. Exploiting tumour hypoxia in cancer treatment. Nat Rev Cancer. 2004; 4: 437-47.
14. Li Y, Sun Y, Li J, Su Q, Yuan W, Dai Y, et al. Ultrasensitive Near-Infrared Fluorescence-Enhanced Probe forin VivoNitroreductase Imaging. J Am Chem Soc. 2015; 137: 6407-16.
15. Guo T, Cui L, Shen J, Zhu W, Xu Y, Qian X. A highly sensitive long-wavelength fluorescence probe for nitroreductase and hypoxia: selective detection and quantification. Chem Commun (Camb). 2013; 49: 10820-2.
16. Okuda K, Okabe Y, Kadonosono T, Ueno T, Youssif BG, Kizaka-Kondoh S, et al. 2-Nitroimidazole-tricarbocyanine conjugate as a near-infrared fluorescent probe for in vivo imaging of tumor hypoxia. Bioconjug Chem. 2012; 23: 324-9.
17. Wardman P, Clarke ED, Hodgkiss RJ, Middleton RW, Parrick J, Stratford MR. Nitroaryl compounds as potential fluorescent probes for hypoxia. I. Chemical criteria and constraints. Int J Radiat Oncol Biol Phys. 1984; 10: 1347-51.
18. Hodgkiss RJ, Jones GW, Long A, Middleton RW, Parrick J, Stratford MR, et al. Fluorescent markers for hypoxic cells: a study of nitroaromatic compounds, with fluorescent heterocyclic side chains, that undergo bioreductive binding. J Med Chem. 1991; 34: 2268-74.
19. Dai M, Zhu W, Xu Y, Qian X, Liu Y, Xiao Y, et al. Versatile Nitro-Fluorophore as Highly Effective Sensor for Hypoxic Tumor Cells: Design, Imaging and Evaluation. J Fluoresc. 2008; 18: 591-7.
20. Begg AC, Hodgkiss RJ, McNally NJ, Middleton RW, Stratford MRL, Terry NHA. Fluorescent markers for hypoxic cells: a comparison of two compounds on three cell lines. The British Journal of Radiology. 1985; 58: 645-54.
21. Tanabe K, Hirata N, Harada H, Hiraoka M, Nishimoto S-i. Emission under Hypoxia: One-Electron Reduction and Fluorescence Characteristics of an Indolequinone–Coumarin Conjugate. ChemBioChem. 2008; 9: 426-32.
22. Zhu W, Dai M, Xu Y, Qian X. Novel nitroheterocyclic hypoxic markers for solid tumor: Synthesis and biological evaluation. Biorg Med Chem. 2008; 16: 3255-60.
23. Cui L, Zhong Y, Zhu W, Xu Y, Du Q, Wang X, et al. A New Prodrug-Derived Ratiometric Fluorescent Probe for Hypoxia: High Selectivity of Nitroreductase and Imaging in Tumor Cell. Org Lett. 2011; 13: 928-31.
24. Xu K, Wang F, Pan X, Liu R, Ma J, Kong F, et al. High selectivity imaging of nitroreductase using a near-infrared fluorescence probe in hypoxic tumor. Chem Commun (Camb). 2013; 49: 2554-6.
25. Chevalier A, Zhang Y, Khdour OM, Kaye JB, Hecht SM. Mitochondrial Nitroreductase Activity Enables Selective Imaging and Therapeutic Targeting. J Am Chem Soc. 2016; 138: 12009-12.
26. Tao Z, Hong G, Shinji C, Chen C, Diao S, Antaris AL, et al. Biological Imaging Using Nanoparticles of Small Organic Molecules with Fluorescence Emission at Wavelengths Longer than 1000 nm. Angewandte Chemie (English Edition). 2013; 52: 13002-6.
27. Hong G, Diao S, Antaris AL, Dai H. Carbon Nanomaterials for Biological Imaging and Nanomedicinal Therapy. Chem Rev. 2015; 115: 10816-906.
28. Won N, Jeong S, Kim K, Kwag J, Park J, Geol KS, et al. Imaging depths of near-infrared quantum dots in first and second optical windows. Mol Imaging. 2012; 11: 1-2.
29. Hong G, Lee JC, Robinson JT, Raaz U, Xie L, Huang NF, et al. Multifunctional in vivo vascular imaging using near-infrared II fluorescence. Nat Med. 2012; 18: 1841.
30. Hong G, Antaris AL, Dai H. Near-infrared fluorophores for biomedical imaging. Nat Biomed Eng. 2017; 1: 0010.
31. Journal of American ScienceIverson NM, Barone PW, Shandell M, Trudel LJ, Sen S, Sen F, et al. In vivo biosensing via tissue-localizable near-infrared-fluorescent single-walled carbon nanotubes. Nat Nanotechnol. 2013; 8: 873-80.
32. Hu YL, Jahangiri A, De Lay M, Aghi MK. Hypoxia-induced tumor cell autophagy mediates resistance to anti-angiogenic therapy. Autophagy. 2012; 8: 979-81.
33. Noman M, Janji B, Moer K, Pierson S, Buart S, Berchem G, et al. Role of hypoxia induced autophagy in the resistance of tumor cells to CTL-mediated specific lysis. (95.11). J Immunol. 2010; 184: 95.11.
34. Meng Y, Wang S, Li C, Qian M, Yan X, Yao S, et al. Photothermal combined gene therapy achieved by polyethyleneimine-grafted oxidized mesoporous carbon nanospheres. Biomaterials. 2016; 100: 134-42.
35. Guo L, Yan DD, Yang D, Li Y, Wang X, Zalewski O, et al. Combinatorial Photothermal and Immuno Cancer Therapy Using Chitosan-Coated Hollow Copper Sulfide Nanoparticles. Acs Nano. 2014; 8: 5670–81.
36. Wang S, Huang P, Nie L, Xing R, Liu D, Wang Z, et al. Single continuous wave laser induced photodynamic/plasmonic photothermal therapy using photosensitizer-functionalized gold nanostars. Adv Mater. 2013; 25: 3055-61.
37. Jung HS, Lee JH, Kim K, Koo S, Verwilst P, Sessler JL, et al. A Mitochondria-Targeted Cryptocyanine-Based Photothermogenic Photosensitizer. J Am Chem Soc. 2017; 139: 9972-8.
38. O'Neal DP, Hirsch LR, Halas NJ, Payne JD, West JL. Photo-thermal tumor ablation in mice using near infrared-absorbing nanoparticles. Cancer Lett. 2004; 209: 171-6.
39. Lal S, Clare SE, Halas NJ. Nanoshell-Enabled Photothermal Cancer Therapy: Impending Clinical Impact. Acc Chem Res. 2008; 41: 1842-51.
40. Melancon MP, Zhou M, Li C. Cancer Theranostics with Near-Infrared Light-Activatable Multimodal Nanoparticles. Acc Chem Res. 2011; 44: 947-56.
41. Okuda K, Okabe Y, Kadonosono T, Ueno T, Youssif BGM, Kizaka-Kondoh S, et al. 2-Nitroimidazole-Tricarbocyanine Conjugate as a Near-Infrared Fluorescent Probe for in Vivo Imaging of Tumor Hypoxia. Bioconjug Chem. 2012; 23: 324-9.
42. Raleigh JA, Chou SC, Arteel GE, Horsman MR. Comparisons among pimonidazole binding, oxygen electrode measurements, and radiation response in C3H mouse tumors. Radiat Res. 1999; 151: 580-9.
43. Varia MA, Calkinsadams DP, Rinker LH, Kennedy AS, Novotny DB, Jr FW, et al. Pimonidazole: a novel hypoxia marker for complementary study of tumor hypoxia and cell proliferation in cervical carcinoma. Gynecol Oncol. 1998; 71: 270-7.
44. Yang D, Tian HY, Zang TN, Li M, Zhou Y, Zhang JF. Hypoxia imaging in cells and tumor tissues using a highly selective fluorescent nitroreductase probe. Sci Rep. 2017; 7: 9174.
45. Knox HJ, Hedhli J, Kim TW, Khalili K, Dobrucki LW, Chan J. A bioreducible N-oxide-based probe for photoacoustic imaging of hypoxia. Nat Comm. 2017; 8: 1794.
46. O'Connor LJ, Mistry IN, Collins SL, Folkes LK, Brown G, Conway SJ, et al. CYP450 Enzymes Effect Oxygen-Dependent Reduction of Azide-Based Fluorogenic Dyes. ACS Cent Sci. 2017; 3: 20-30.
47. Kiyose K, Hanaoka K, Oushiki D, Nakamura T, Kajimura M, Suematsu M, et al. Hypoxia-Sensitive Fluorescent Probes for in Vivo Real-Time Fluorescence Imaging of Acute Ischemia. J Am Chem Soc. 2010; 132: 15846-8.
48. Takahashi S, Piao W, Matsumura Y, Komatsu T, Ueno T, Terai T, et al. Reversible Off-On Fluorescence Probe for Hypoxia and Imaging of Hypoxia-Normoxia Cycles in Live Cells. J Am Chem Soc. 2012; 134: 19588-91.
49. Piao W, Tsuda S, Tanaka Y, Maeda S, Liu FY, Takahashi S, et al. Development of Azo-Based Fluorescent Probes to Detect Different Levels of Hypoxia. Angew Chem Int Ed Engl. 2013; 52: 13028-32.
50. Patterson LH, McKeown SR. AQ4N: a new approach to hypoxia-activated cancer chemotherapy. Br J Cancer. 2000; 83: 1589-93.
51. Bashkatov AN, Genina EA, Kochubey VI, Tuchin VV. Optical properties of human skin, subcutaneous and mucous tissues in the wavelength range from 400 to 2000 nm. J Phys D: Appl Phys. 2005; 38: 2543-55.
52. Hong G, Zou Y, Antaris AL, Diao S, Wu D, Cheng K, et al. Ultrafast fluorescence imaging in vivo with conjugated polymer fluorophores in the second near-infrared window. Nat Comm. 2014; 5: 4206.
53. Hong G, Lee JC, Jha A, Diao S, Nakayama KH, Hou L, et al. Near-Infrared II Fluorescence for Imaging Hindlimb Vessel Regeneration With Dynamic Tissue Perfusion Measurement. Circ Cardiovasc Imaging. 2014; 7: 517-25.
54. Welsher K, Sherlock SP, Dai H. Deep-tissue anatomical imaging of mice using carbon nanotube fluorophores in the second near-infrared window. Proc Natl Acad Sci USA. 2011; 108: 8943–8.
55. Xu J, Sun S, Li Q, Yue Y, Li Y, Shao S. A rapid response "Turn-On" fluorescent probe for nitroreductase detection and its application in hypoxic tumor cell imaging. Analyst. 2015; 140: 574-81.
56. Li Y, Sun Y, Li J, Su Q, Yuan W, Dai Y, et al. Ultrasensitive near-infrared fluorescence-enhanced probe for in vivo nitroreductase imaging. J Am Chem Soc. 2015; 137: 6407-16.

57. Jiang Y, Upputuri PK, Xie C, Lyu Y, Zhang L, Xiong Q, et al. Broadband Absorbing Semiconducting Polymer Nanoparticles for Photoacoustic Imaging in Second Near-Infrared Window. Nano Lett. 2017; 17: 4964-49369.
58. Jiang Y, Li J, Zhen X, Xie C, Pu K. Dual-Peak Absorbing Semiconducting Copolymer Nanoparticles for First and Second Near-Infrared Window Photothermal Therapy: A Comparative Study. Adv Mater. 2018; 30: 1705980.
59. Jiang Y, Pu K. Molecular Fluorescence and Photoacoustic Imaging in the Second Near-Infrared Optical Window Using Organic Contrast Agents. Adv Biosys. 2018; 2: 1700262.
60. Koder RL, Miller AF. Steady-state kinetic mechanism, stereospecificity, substrate and inhibitor specficity of Enterobacter cloacae nitroreductase. Biochim Biophys Acta Biochim Biophys Acta. 1998; 1387: 395-405.
61. Zheng X, Mao H, Huo D, Wu W, Liu B, Jiang X. Successively activatable ultrasensitive probe for imaging tumour acidity and hypoxia. Nat Biomed Eng. 2017; 1: 0057.
62. Zheng X, Wang X, Mao H, Wu W, Liu B, Jiang X. Hypoxia-specific ultrasensitive detection of tumours and cancer cells in vivo. Nat Comm. 2015; 6: 5834.
63. Wang Y, Xie Y, Li J, Peng ZH, Sheinin Y, Zhou J, et al. Tumor-Penetrating Nanoparticles for Enhanced Anticancer Activity of Combined Photodynamic and Hypoxia-Activated Therapy. ACS Nano. 2017; 11: 2227-38.